Reflection spectroscopy of $ZrSe_3$-type family of layer compounds in the vacuum ultraviolet region

F. S. Khumalo* and H. P. Hughes
Physics and Chemistry of Solids, Cavendish Laboratory, Madingley Road, Cambridge CB3 0HE, England
(Received 14 March 1980)

Near-normal-incidence vacuum ultraviolet reflectivity spectra, in the photon energy range 3.7 to 14 eV (in some cases the range is extended to 30 eV) have been obtained from basal faces of freshly cleaved single crystals of the layered trisulphides, triselenides, and tritellurides of titanium, zirconium, and hafnium (with the exception of the hitherto unreported $TiSe_3$ and $TiTe_3$). The spectra are interpreted using physical and chemical arguments as well as simple molecular-orbital ideas. Chemical trends in the series S→Se→Te are manifest in the presented spectra. Using the information inferred from these spectra as well as the information on these materials available in the literature to date, band-structure models for these $ZrSe_3$-type compounds have been proposed and are presented in this paper. Unlike their sister compounds (the $ZrSe_2$-type layer compounds), the $ZrSe_3$-type materials are envisaged as having predominantly dimerized main valence and conduction bands.

I. INTRODUCTION

Over the past two decades, layer compounds with the chemical formula MX_2 (where $M \equiv$ Group IVA or VA or VIA transition metal and X is one of the chalcogens S, Se, Te) have been the focus of much optical study and the diversity of their physical properties is now known to be due to the existence, within the electronic bonding, of a narrow band formed from the d_{z^2} orbitals of the transition metal; the degree to which this band is filled in the various MX_2 layer compounds (MoS_2 is an archetype) determines their physical properties [e.g., MoS_2 (Group VIA) is a semiconductor while $NbSe_2$ (Group VA) is metallic and a superconductor]. In sharp contrast, despite numerous crystallographic, magnetic, and electrical studies, only limited knowledge is at hand concerning the optical properties of another interesting class of layer compounds—the Group IVA trichalcogenides with the chemical formula MX_3 (where here $M \equiv$ Ti, Zr, Hf; and $X =$ S, Se, Te). $ZrSe_3$ is an archetype of these materials.

These MX_3 layer compounds crystallize monoclinically (space group P_{2_1}/M) in fibrous strands or filamentary ribbon-shaped platelets. A linear chain of metal atoms is parallel to the b axis (the growth axis), and six chalcogen (X) atoms surround each metal atom forming distorted trigonal prisms (see Figs. 1–3). The distance between metal atoms along the b axis is much shorter than the interprism distances.[1] These structures have the analogy of a bundle of metallic chains each with an insulating sheath. The platelets run parallel to the b crystallographic axis and are displaced from neighboring columns by half the unit cell along the b axis. The van der Waals sulphur-sulphur bonds are in a plane perpendicular to the columns and the van der Waals gap is nearly perpendicular to the c axis. There are two formula units of $ZrSe_3$ within the cell (see Figs. 2 and 3). The cleavage plane is parallel to the a-b plane (see Fig. 1).

Kronert and Plieth,[1] Hamann,[2] McTaggart and Wadsley,[3] Bear and McTaggart,[4] and McTaggart[5] have done extensive work on the synthesis and crystallographic structure determination of these $ZrSe_3$-type materials. Zirconium and hafnium readily form all the three trichalcogenides but titanium forms only a trisulphide; $TiSe_3$ and $TiTe_3$ have not been reported in the literature. All the trichalcogenides of Group IVA have been found to be isomorphous with $ZrSe_3$ (monoclinic symmetry).[6]

The structural features described above and the observations that the trisulphides and triselenides

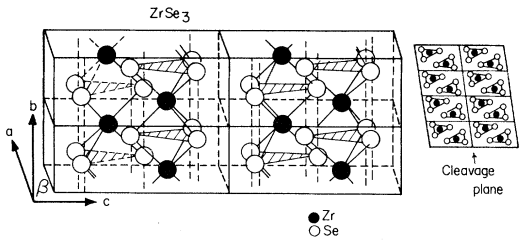

FIG. 1. Three-dimensional crystal structure (Ref. 1) of $ZrSe_3$. The layer-type lattices have the metal ions in the center of the distorted trigonal prisms which share trigonal faces thus forming isolated columns. The columns (or platelets) run parallel to the b crystallographic axis and are displaced from the neighboring columns by one-half the unit cell along the b axis. Zr-Se distance in prism = 2.74 Å. Zr-Se distance between stacks = 2.87 Å; Zr-Zr distance along b axis = 3.77 Å.

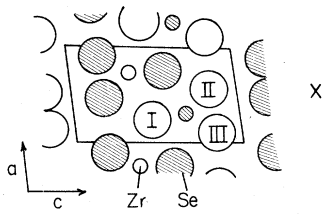

FIG. 2. The structure of $ZrSe_3$ projected along the b axis. Atoms indicated by unhatched circles are at the $y=\frac{1}{4}$ mirror plane and atoms indicated by hatched circles are at the $y=\frac{3}{4}$ mirror plane. The outlines of the unit cell are indicated.

of these $ZrSe_3$-type materials are diamagnetic[6,7] semiconductors[5,8,9] have prompted some workers[1,10] to regard these MX_3 compounds as $M^{4+}X^{2-}(X_2)^{2-}$. However, this formula should not be taken to mean that these compounds are fully ionic because the Zr–Se bonds will be partly covalent.

The earliest reported optical work on the $ZrSe_3$-type materials is that by Grimmeiss *et al.*[8] where optical absorption was performed on crystals of TiS_3, ZrS_3, HfS_3, and $ZrSe_3$. The direct energy gap values of 0.9, 2.2, 2.8, and 1.2 eV were obtained by Grimmeiss *et al.*[8] for TiS_3, ZrS_3, HfS_3, and $ZrSe_3$ respectively. Diffuse reflectance spectra measurements have been performed in TiS_3, ZrS_3, HfS_3, $ZrSe_3$, and $HfSe_3$ by Brattas and Kjekshus.[6] Using an extrapolation method, Brattas and Kjekshus[6] obtained the following values for the band gaps: 0.83, 1.95, 1.11, 1.91, and 1.02 eV for TiS_3, ZrS_3, HfS_3, $ZrSe_3$, and $HfSe_3$, respectively. The most reliable optical work on these materials is that by Schairer and Shafer[9] who performed optical absorption measurements on single crystals of ZrS_3 and HfS_3. Both compounds were found to be semiconductors with band-gap energies of ~2.8 and 3.1 eV, respectively. Furthermore, Schairer and Shafer[9] noticed that both compounds exhibit pronounced dichroism in the energy range of their intrinsic absorption edges. The results of absorption experiments seem to indicate that Group IVA trichalcogenides (except for TiS_3) are probably wide-band semiconductors.

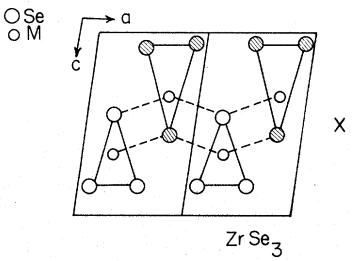

FIG. 3. The structure of $ZrSe_3$ projected along the b axis showing the metal-metal or chalcogen-chalcogen chains.

Photoemission spectra have been obtained on ZrS_3 and $ZrSe_3$ (and also on ZrS_2 and $ZrSe_2$) by Jellinek *et al.*[10] and their results seem to reveal that the valence band of ZrS_3 is split into two and also that the core levels of ZrS_2 lie at slightly higher binding energies than those in ZrS_3.

From this short survey, it is clear that optical work on these $ZrSe_3$-type materials is still very sparse. While the optical properties (mainly in the visible region) of these Group IVA transition metal trichalcogenides have already been studied (to a limited extent), as we have already mentioned earlier, systematic measurements in the vacuum ultraviolet (vuv) region are not yet reported. The wealth of information (especially about the conduction-band states) a systematic vuv study can reveal has motivated this present study.

In this paper, near-normal-incidence reflectivity spectra, in the photon energy range 3.7–14 eV (and for ZrS_3, $ZrSe_3$, and $HfSe_3$, the energy range was extended to 30 eV) from basal faces of freshly cleaved single crystals of the Group IVA trichalcogenides are reported. Measurements were made at room and liquid-nitrogen temperatures, and in some cases, considerable sharpening of many features of the spectra was observed at the lower temperature.

II. EXPERIMENTAL ASPECTS

Single crystals of TiS_3, ZrS_3, $ZrSe_3$, $ZrTe_3$, HfS_3, $HfSe_3$, and $HfTe_3$ were all grown by the now widely used method of vapor transport. Iodine was found to be the most ideal transport agent in growing these $ZrSe_3$-type crystals. All the MX_3 compounds form a layer lattice and twins are easily created in these materials.[1]

Two types of equipment were used in this work. For the photon energy range 3.7 to 14 eV, the vacuum ultraviolet apparatus at the Cavendish Laboratory, Cambridge, England was used. This equipment consists of a vuv light source, a Hilger and Watts E760 vacuum monochromator with a 1-m Bausch and Lomb concave grating ruled at 590 lines mm^{-1}, and an appropriate specimen chamber. Light from the monochromator exit slit is divided into two parts. The center portion of the light falls directly onto the sample which is mounted on a copper "cold finger" at the base of a Dewar. The Dewar is surrounded by a liquid-nitrogen-cooled copper radiation shield which serves as a very effective cold trap for contaminants (e.g., water vapor, dust particles) which would otherwise reach the freshly cleaved

sample surface. The remainder of the incident light is collected by two flexible fiber-optic light guides. Light reflected from the sample falls onto the end of a rotatable fiber light guide. The front ends of the light guides are thinly and evenly coated with sodium salicylate phosphor, and the "reference" (reference intensity is that obtained when the sample is moved out of the path of the probing light) and reflected intensities are detected at the other ends by a pair of matched EMI6256S photomultipliers mounted inside the specimen chamber. The photomultipliers are cooled by partial thermal contact with the radiation shield. Thus both incident and reflected intensities can be monitored simultaneously, and time-dependent fluctuations in the light source output virtually eliminated. The rotatable light guide arrangement permits the reflectivity measurements at any angle of incidence greater than 5°, and furthermore, this arrangement allows transmission measurements to be made. Measurements are normalized with the sample moved out of the light path and the rotatable light guide turned to face the incident beam. With "optically flat" crystal surfaces, the reflectivity measurements should, ideally, be absolute. However, surface irregularities produce scatter in the reflected beam and it is not certain that all the reflected light is collected by the rotatable light guide. Further discrepancies are introduced by variations of the quantum efficiency over the areas of the phosphor coating and the photomultiplier photocathode, so the data presented in this work should not be regarded as accurately absolute. (There is probably a 5–10% deviation from the absolute.) The light beam is chopped at the monochromator entrance slit by a piezoelectrically vibrated blade driven at resonance (157 Hz) by a square-wave generator; the outputs from the photomultipliers are fed into two 100-MHz-bandwidth preamplifiers, and from the preamplifiers the outputs are fed into two discriminators and then into four gated digital scalers. All the wavelength, signal, and normalization run information is sent from the photon counter directly onto a floppy disc of a minicomputer. All the data analysis was done on the minicomputer and the subsequent spectra were displayed first on the oscilloscope and then finally on the X-Y chart recorder.

The range 3.7 to 14 eV was covered using two laboratory light sources: A commercial deuterium arc lamp (60 V, $\frac{1}{2}$ A) having a quartz envelope produces a smooth continuum at photon energies below the quartz cutoff (~1650 Å), while at higher energies, a hot-cathode hydrogen glow discharge lamp (~200 V, 3 A, optimum pressure ~0.2 Torr) based on a design of Eastman and Donelon,[11] operated windowless, provides a many-lined spectrum falling off rapidly in intensity above 12 eV. In the lined region of the H_2 lamp spectrum, the light intensity varies rapidly with wavelength over several orders of magnitude, so it is not possible to make a continuous wavelength scan; data are therefore recorded at fixed wavelength points. These points are determined, for convenience, by the markings on the monochromator stepping-motor-driven wavelength drum rather than at line intensity peaks; therefore, readings are generally taken on the sides of atomic lines. The line intensities are particularly sensitive to lamp operating conditions (e.g., filament life, discharge current, pressure, etc.) and the dual-beam monitoring system is invaluable here in reducing these fluctuations.[12] Also, the background noise from the photomultiplier (e.g., thermal emission from photomultiplier dynodes, etc.) is eliminated by the synchronous sampling of data and as a result, the signal-to-noise ratio varies from 10^4 in the low light intensity regions to 10^6 in the regions where there is a lot of light. The energy resolution is everywhere better than the point intervals. All spectra were repeated several times to check reproducibility. All spectra presented in this paper were highly reproducible. Further details on the Cambridge vacuum ultraviolet equipment can be found in a paper by Hughes and Liang.[13]

The range 10 to 30 eV was covered by use of a soft x-ray source at the Synchrotron Radiation Facility (SRF) NINA at Daresbury Laboratory Warrington, Cheshire, England. At Daresbury, spectroscopists in the SRF were, for the most part, parasitic upon high-energy physics experiments. Radiation emitted during the electron acceleration shines down beam tubes attached to the ring-shaped chamber in which the electrons are accelerated. The axis of each of these tubes meets tangentially a point in the electron orbit within a bending magnet and the diameters of these tubes increase in size from ~0.1 m near the magnet point to 0.28 m at their ends in the SRF. Each beam tube enters the SRF via a remotely vacuum-enclosed beam shutter made of lead, two feet thick. This shutter thickness is enough to isolate the experimental area of the SRF when NINA carries a pulsed (circulating) electron beam.[14]

The experimental setup and procedure at the SRF was similar in every way to that used in the Cambridge vuv equipment described earlier—i.e., a light source (NINA in this case), a grating (vertical Wordsworth mount), a sample and detector (channeltrons)—all under vacuum. Then a CAMAC photon counter was used to count photons from the channeltrons. All detailed description and mode

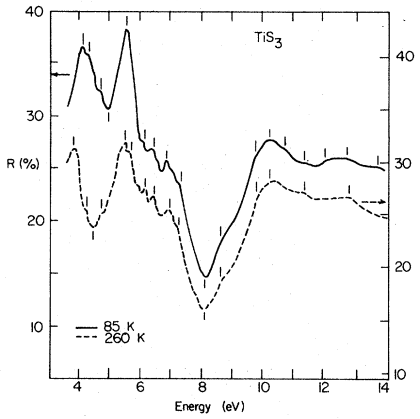

FIG. 4. Vacuum ultraviolet reflectivity spectrum of TiS_3.

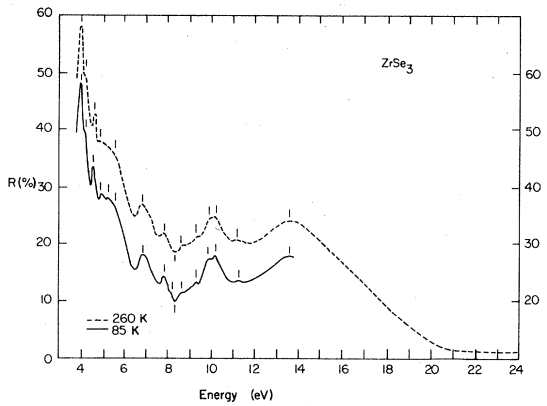

FIG. 6. Vacuum ultraviolet reflectivity spectrum of $ZrSe_3$.

of operation of each piece of equipment used at the SRF can be found in Bourdillon's Ph.D. thesis.[15] Here it will suffice to mention that a resolution of 0.1 Å could be achieved on NINA. The monochromator was evacuated to a pressure of $\sim 10^{-8}$ Torr or better using a turbomolecular pump. Five filters (LiF, Sn, indium, and Al) were used to cut out second-order light. The channeltrons used were a Mullard B419BL. The channeltrons needed a vacuum of at least 10^{-4} Torr to work in and they were placed inside the sample chamber. One great advantage of these detectors (over photomultipliers) is that they are solar blind and therefore are insensitive to stray visible light.

III. RESULTS AND DISCUSSION

Near-normal-incidence ($i \leq 10°$) reflectivity spectra of freshly cleaved (in air) basal layer faces of single crystals of TiS_3, ZrX_3, and HfX_3 (where X = S, Se, Te) measured at 85 and 260 K, are shown in Figs. 4–10, respectively. At room temperature, the energy range for $ZrSe_3$, ZrS_3, and $HfSe_3$ were extended to 30 eV by use of NINA. For $ZrSe_3$, ZrS_3, and $HfSe_3$, the reflectivity just tails off rapidly to zero after ~24 eV, and so, to show more structure at low photon energies, the energy range for $ZrSe_3$, ZrS_3, and $HfSe_3$ spectra has been truncated to 24.0 eV. The energies of features (in eV) on the spectra presented are shown in Tables I, II, and III. The reproducible features on the spectra are indicated by short vertical lines.

In the following paragraphs, the following observations will be discussed: (i) The spectrum of TiS_3 exhibits sharp reflectivity minimum between 4 and 5 eV, and also between 7 and 8 eV. (ii) The TiS_3 spectrum is clearly dissimilar (in the same photon energy range) from the spectra of Zr or Hf compounds. (iii) If one studies the spectra of ZrX_3 and HfX_3 (X = S, Se, Te) it is immediately apparent that there are gross similarities between the spectra of Zr and Hf compounds. (iv) If

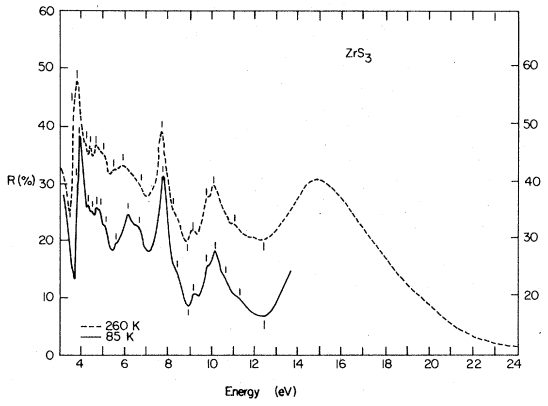

FIG. 5. Vacuum ultraviolet reflectivity spectrum of ZrS_3.

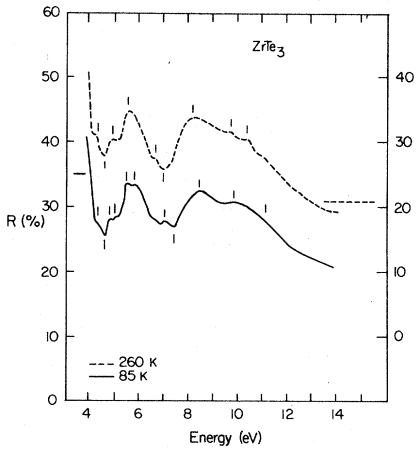

FIG. 7. Vacuum ultraviolet reflectivity spectrum of $ZrTe_3$.

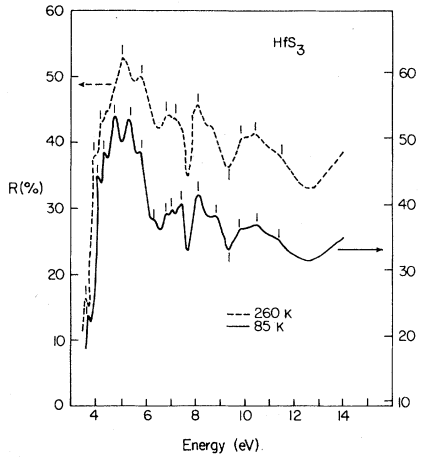

FIG. 8. Vacuum ultraviolet reflectivity spectrum of HfS_3.

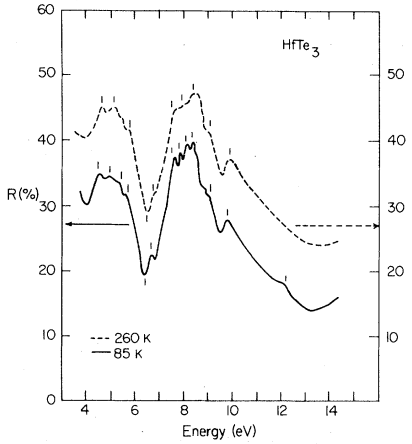

FIG. 10. Vacuum ultraviolet reflectivity spectrum of $HfTe_3$.

the spectra of MS_3, MSe_3, and MTe_3 (where M is Zr or Hf) are superposed, there is an expected general shift, in the reflectivity features, to lower photon energies as one goes down the chalcogen series group (S → Se → Te) in the Periodic Table of elements. (v) Using both polarized (NINA) and partially polarized light (Cambridge vuv equipment), no dichroism was observed in the Group IVA trichalcogenides in the ranges 3.7 to 14 eV and 10 to 30 eV.

A. Discussion

The marked drop in the reflectivity near 8 eV on the TiS_3 spectrum (Fig. 4) is reminiscent of a collective plasma resonance observed in the vuv reflectivity spectra of Mo dichalcogenides.[13] This marked minimum often occurs after the exhaustion of a region of interband transitions. This minimum often marks a well-defined window in the optical joint density of states. We suggest here that the depth of the minimum (~25%) on the TiS_3 reflectivity spectrum is representative of the degree of overlap between two absorption regions on either side of the window. It is further suggested that the observed collective plasma resonance-like minimum in the vuv reflectivity spectrum of TiS_3 probably arises from a gap in the conduction-band density of states of TiS_3 (see proposed band model later). The distinct minimum in the vuv reflectivity spectrum of TiS_2 was interpreted this way by Hughes and Liang.[16] Incidently, we have also observed that the spectra of TiS_2 and TiS_3 are remarkably similar. This similarity will be discussed in our next paper on $ZrSe_2$- and $ZrSe_3$-type compounds.

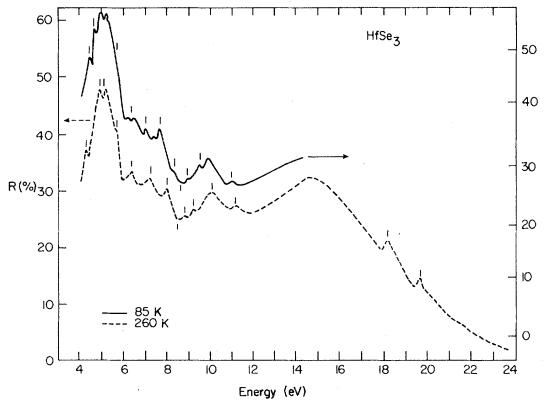

FIG. 9. Vacuum ultraviolet reflectivity spectrum of $HfSe_3$.

TABLE I. Features (in eV) on the TiS_3 spectrum.

260 K	85 K
	13.75
12.76	12.80
	12.30
11.36	11.46
	10.80
10.39	10.35
9.96	9.83
9.04	8.76
8.09[a]	8.18[a]
7.22	7.29
6.97	6.83
6.38	6.39
6.15	6.10
5.66	5.53
5.40	4.94
4.68	4.65
4.39	4.30
4.25	4.08
3.89	

[a] Indicates distinct minimum on the spectrum.

TABLE II. Features (in eV) on the ZrS_3, $ZrSe_3$, and $ZrTe_3$ spectra.

ZrS_3		$ZrSe_3$		$ZrTe_3$	
260 K	85 K	260 K	85 K	260 K	85 K
12.42	12.50				
11.22	11.22	11.22	11.36		11.06
10.58	10.64	10.23	10.35	10.35	10.21
10.18	10.23	9.85	10.06		
9.80	10.17	9.22	9.31	9.75	
9.17	9.26	8.58	8.70		
8.91	8.95	8.28	8.31		
8.31	8.39		8.17	8.03	8.36
7.76	7.79	7.69	7.82	7.05	7.01
6.74	6.80	6.70	6.97	6.67	6.00
5.89	5.64				5.64
5.56	5.45	5.44	5.23	5.43	5.36
5.01	4.90	4.76	5.01	4.80	5.05
4.74	4.75				4.84
4.41	4.50	4.52	4.59	4.59	4.63
4.16	4.39	4.16	4.23	4.23	
3.91	3.98	3.93	3.97		
3.76	3.83				
3.56	3.69				

The striking dissimilarity between the spectra of ZrS_3 or HfS_3 compounds and TiS_3 can be explained in the following way: Let us consider the effect of the metal-metal distances (in Å) within the layers (for the three compounds) and the size of the metal ions (the 4+ ionic radii) on the band

TABLE III. Features (in eV) on the HfS_3, $HfSe_3$, and $HfTe_3$ spectra.

HfS_3		$HfSe_3$		$HfTe_3$	
260 K	85 K	260 K	85 K	260 K	85 K
		19.90			
		18.10			
					12.17
11.32	11.45	11.15	11.28		
10.96	10.89	10.00	9.94	10.08	9.85
9.96	9.98				
9.31	9.40	9.26	9.32	9.19	9.13
	9.17	8.82	8.94	8.66	8.73
8.38	8.38			8.16	8.17
7.92	7.92	7.92	7.88	7.96	7.96
7.58	7.64	7.29	7.44		
7.12	7.24			6.95	7.03
6.79	6.79			6.75	6.54
6.57	6.57	6.32	6.32		
6.09	6.11			5.88	5.96
5.76	5.79	5.65	5.68		5.19
	4.94			4.84	4.99
4.83	4.83			4.58	4.61
4.73	4.76	4.35	4.35		
4.40	4.48				
3.82	3.86				

TABLE IV. Metal-metal distances and lattice constants of the trisulphides of titanium, zirconium, and hafnium.

Compound	"b" lattice constant (Å)	$r_{M^{4+}}$	Atomic weight (M)
TiS_3	3.400	0.68	47.90
ZrS_3	3.620	0.79	91.22
HfS_3	3.595	0.79	178.49

structure of each compound (see Table IV). The metal-metal distances in these materials are given by the values of the "b" axis (the axis of growth in these monoclinic crystals). The b lattice constants given in Table IV are quoted from Brattas and Kjekshus,[6] the 4+ ionic radii are quoted from Ahrens.[17] The degree of metal-metal overlap and hence the forms of the metal-orbital based $d(M)$-$p(X\text{-}X)^*$ and $s(M)$ conduction bands [$(X\text{-}X)^*$ are antibonding S–S pairs] are largely determined by the size of both the b lattice constant and the 4+ ionic radius of the transition metal in the compound. In Table IV we observe that there is relatively a big change in the magnitude of the b lattice constant in going from TiS_3 to ZrS_3 or HfS_3. Similarly, it is true for the 4+ ionic radii. The differences in these parameters account for the striking difference between the reflectivity spectra of Ti and Zr or Hf compounds for the following reasons:

(a) The effect of the chalcogen ligand field on the metal d states increases with increasing atomic number; the decreasing metal electronegativity increases the charge transfer to the chalcogen and hence increases the ligand field. The outer orbital radii (1.51 Å) of Zr and Hf (Ref. 18) are slightly larger than the corresponding Ti (1.36 Å) outer orbital radius and so are likely to be more affected by the chalcogen ligand field. These factors would lead to wider overall $d(M)$-$p(X\text{-}X)^*$ conduction bands for the Zr or Hf compounds as compared with the Ti compounds thus pushing the upper part of the Zr or Hf compound conduction band up into the energy region of the metal s conduction band and so increasing the likelihood of overlap of bands, more so in Zr or Hf compounds, than in Ti compounds. Furthermore, since Ti is a comparatively small ion, the effect of the ligand field on it will be less than in Hf or Zr.

(b) For free atoms with the same outer electronic configuration the energy separation between nd and $(n+1)s$ levels decreases with increasing principal quantum number n. The Zr $4d$ and $5s$ levels will therefore be less well separated than the Ti $3d$ and $4s$ levels and this will carry over into the band structures (and to the

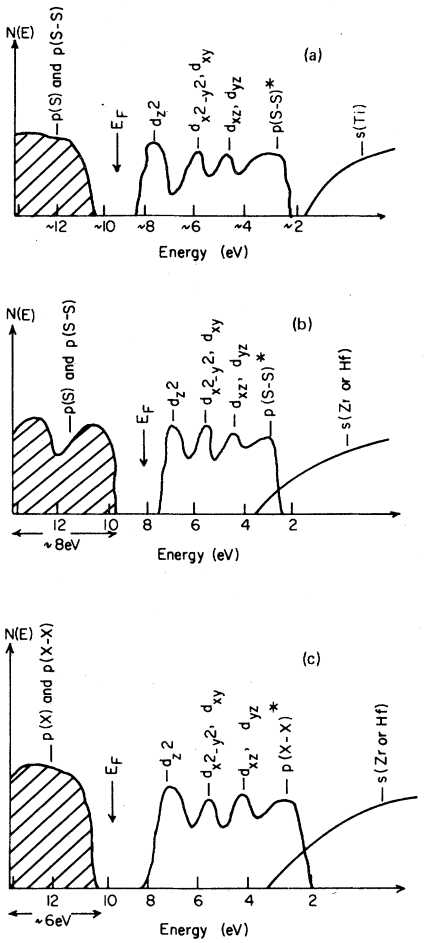

FIG. 11. (a) Proposed band-structure model for TiS_3. (b) Proposed band-structure model for ZrS_3 or HfS_3. (c) Proposed band-structure model for ZrX_3 or HfX_3 where X = Se, Te.

reflectivity spectra) and thus increase the possibility of overlap, more so in Zr or Hf compounds than in Ti compounds.

(c) Because of the larger b lattice constant value for ZrS_3 (3.602 Å) as compared with that for TiS_3 (3.400 Å), as shown in Table IV, and furthermore because of the large increase in the outer orbital radii of Zr or Hf, there will be greater metal-metal overlap and hence broader $d(M)$-$p(X$-$X)$* (hence less gaps between conduction bands) and s conduction bands in ZrS_3 or HfS_3 than in TiS_3.

Therefore because of the above reasons (and hence the dissimilarities in spectra between ZrS_3 or HfS_3, and TiS_3) we would expect the density-of-states distributions (hence the energy-band structures) to be different.

In view of the above chemical arguments, a band model for TiS_3 [Fig. 11(a)] has been drawn with a clear separation between the d(Ti)-p(S–S)* and s(Ti) conduction bands. The drop in reflectivity near 4 eV on the TiS_3 spectrum is probably due to exhaustion of optical transitions from p(S) and p(S-S) to $d_{z^2}(M)$ which is probably at the bottom of the main conduction band in TiS_3.

It is noticeable from Figs. 5, 6, and 7 that there is an apparent general shift of reflectivity features to lower energies as one goes across the series $ZrS_3 \rightarrow ZrSe_3 \rightarrow ZrTe_3$ (similarly for Hf compounds). For instance, to superpose the $ZrSe_3$ spectrum onto the ZrS_3 spectrum, one needs to shift, to high energies, the $ZrSe_3$ spectrum (by ~ 0.6 eV); to superpose the spectra of $ZrSe_3$ and $ZrTe_3$, we need to shift the $ZrTe_3$ spectrum, to high energies, by as much as ~ 0.9 eV. These shifts imply that the band structures of the three Zr compounds are very closely similar except that the $ZrSe_3$ conduction bands are ~ 0.6 eV lower with respect to the main ZrS_3 valence band, and similarly for $ZrTe_3$. (A similar treatment for HfS_3, $HfSe_3$, and $HfTe_3$ would produce a similar conclusion.) Furthermore, there seems to be a considerable broadening of reflectivity features in going across the series $S_3 \rightarrow Se_3 \rightarrow Te_3$. The reasons for the shifting of features to low energies and the broadening of features as we go across the chalcogen series S → Se → Te can be understood from the following chemical arguments. Let us consider, again, the metal-metal distances (in Å) within the layers for the three Zr compounds. Also we shall compare the electronegativity values of S, Se, and Te, and also the atomic weight values of these three chalcogens. Table V shows these values.

As mentioned earlier, the metal-metal (b lattice constant values) distances within the layers of a ZrX_3 ($X \equiv$ S, Se, Te) compound determine the Zr-Zr overlap, and hence largely the forms of the

TABLE V. Electronegativities and lattice constants of the trichalcogenides of zirconium.

Compound	Electronegativity of X(= S, Se, Te)	"b" lattice constant (Å)	Chalcogen atomic weight
ZrS_3	2.58	3.62	32.064
$ZrSe_3$	2.55	3.74	78.96
$ZrTe_3$	2.01	3.96	127.60

$d(Zr)$-$p(X$-$X)$* and $s(Zr)$ conduction bands. From Table V, we note that there is a slight change between the trisulphide and triselenide (for the same 4+ ionic radius of Zr), but a much larger increase in the b lattice constant for the tritelluride will result in considerably reduced Zr-Zr overlap and thus tend to produce narrower metal-orbital based conduction bands. However, because Te is a much larger atom than either S or Se, its outer orbitals will be screened (by the inner orbitals) from the positive nucleus thus tending to produce broader metal-orbital based conduction bands in $ZrTe_3$ (see Ref. 19). Also, the decreasing ionicity with increasing chalcogen weight would tend to broaden the metal-orbital based conduction bands by increasing the degree of covalent mixing of the orbitals. The decreasing chalcogen electronegativity across the series S → Se → Te (see Table V) will also reduce the ligand field splitting of the metal d levels and thus produce a narrower overall $d(M)$-$p(X$-$X)$* band. It is clear from Figs. 5–10 that broadening effects dominate as one goes across the series S → Se → Te. Also, the shifting of spectra to low photon energies as one goes across the series $MS_3 \rightarrow MSe_3 \rightarrow MTe_3$ (where M = Zr or Hf) is caused by the decreasing chalcogen electronegativity across the series S → Se → Te.

A detailed assignment of features on the reflectivity spectra of ZrX_3 and HfX_3 compounds presented here is difficult without any calculated band structures of these compounds. With the help of a published density-of-states distribution of $ZrSe_3$ (Ref. 20) and also the information that the valence band in ZrS_3 is split into two distinct bands,[10] schematic band-structure models for ZrS_3 or HfS_3 and ZrX_3 or HfX_3 (X = Se, Te) have been proposed [see Figs. 11(b) to 11(c)] in the light of vuv reflectivity spectra presented in this work. If the spectra of ZrS_3 and $ZrSe_3$ are superposed, allowing for the effect due to the chalcogen electronegativity, it is found that between 4–8 eV the $ZrSe_3$ spectrum merely exhibits a falling edge in reflectivity with increase in photon energy whereas ZrS_3 exhibits a lot of interband transitions. This dissimilarity in spectra at low energies between $ZrSe_3$ and ZrS_3 may be attributed to the fact that the valence band in ZrS_3 is split into two portions and that of $ZrSe_3$ is not.[10] Therefore, at low photon energies, there would be more $p(X) \rightarrow d(M)$ transitions in ZrS_3 than in ZrS_3. The falling edge in reflectivity between 4 and 8 eV in ZrS_3, $ZrSe_3$, and $HfSe_3$ probably indicates that there is some degree of separation of the upper "d" band into two pairs: $d_{xy}, d_{x^2-y^2}$ and d_{xz}, d_{yz} characters. This separation of the upper "d" bands is probably more marked in ZrS_3 than in $ZrSe_3$—hence there would be more interband transitions in ZrS_3 than in $ZrSe_3$. Also, ZrS_3 exhibits fairly sharp minima at about 4 eV, between 5 and 6 eV, at ~7 eV, at ~9 eV, and between 12 and 13 eV. There are also a number of fairly sharp excitoniclike peaks on ZrS_3—such peaks are at 7.76 and 4.16 eV. Obviously, without known values of n_{eff} (the effective number of electrons, per unit cell, taking part in optical transitions), it is difficult to assign, with confidence, the Se (or S or Te) features on the $ZrSe_3$ spectrum to particular transitions using the schematic band-structure models shown in Figs. 11(a)–11(c). The various minima, at both high and low photon energies, on the ZrS_3 spectrum strongly suggest that there is a lot of separation of the "d" bands in the conduction band of this material. If the empty "d" bands in ZrS_3 are slightly separated from $p(S-S)$* as the band-structure model proposed in this work [Fig. 11(c)] suggests, then one is immediately tempted to make the following, as yet, tentative and speculative assignments on the ZrS_3 vuv reflectivity spectrum:

(a) minimum at ~4.61 eV is probably due to exhaustion of $p(X) \rightarrow d_{z^2}(M)$ transitions;

(b) minimum between 5 and 6 eV is probably due to the exhaustion of $p(X)$ to $d(M)_{x^2-y^2}$ or $d(M)_{x,y}$ transitions;

(c) minimum between 6–7 eV is probably due to the exhaustion of $p(X)$ to $d(M)_{x,y}$ or $d(M)_{yz}$ transitions;

(d) minimum at 8–9 eV is probably due to exhaustion of $p(X)$ to $d(M)$ or $p(X-X)$* transitions.

The lowest minimum at 12.50 eV on the ZrS_3 spectrum is probably due to the exhaustion of optical transitions from the $p(X)$ valence band (~8 eV wide)[10] to the top of the main $d(M)$-$p(X-X)$* conduction band and then the onset of $p(X-X)$ or $p(X)$ to $s(Zr)$ transitions. It is worth mentioning that all the transitions in the foregoing arguments have been assumed to originate from the $p(X)$ valence band of ZrS_3 because of a wide valence bandwidth of 8 eV in ZrS_3 (Ref. 10) as compared with a valence width of 6 eV in $ZrSe_3$.[20] It is thus proposed, in this paper, that because of their apparent narrow valence bands, the interband transitions in the $ZrSe_3$ and $HfSe_3$ (and probably $ZrTe_3$ and $HfTe_3$ as well) vuv spectra are representative of conduction-band states while the (apparent) presence of a wide valence band in ZrS_3 (and perhaps in HfS_3) implies that the vuv spectra of these two materials are representative of valence to conduction-band (strong $p \rightarrow s$) transitions.

We would now like to explain the cause of the expected similarity between the reflectivity spectra of Hf and Zr trichalcogenides. Figure 12

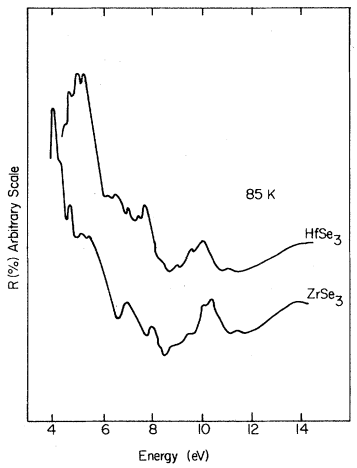

FIG. 12. The spectra of $ZrSe_3$ and $HfSe_3$ compared.

shows the spectra of $ZrSe_3$ and $HfSe_3$ plotted one above the other. There is a striking similarity between the two spectra. The question is: Why? The answer to this question is as follows.

Zr is above Hf in Group IVA of the periodic table of elements. Normally, on descending a group in the periodic table, the covalent and ionic radii increase due to the filling of the extra shells of electrons. Therefore, normally we would expect Hf^{4+} to have a larger ionic radius (or covalent radius) than Zr^{4+}. However, because of the effects of lanthanide contraction amounting to 0.21 Å, both the atomic radii of Zr and Hf (1.45 and 1.44 Å, respectively) and the ionic radii of the Zr^{4+} and Hf^{4+} ions (0.79 Å for each)[17] are virtually identical. This lanthanide contraction effect makes the chemical behavior of the compounds of these two elements (Zr and Hf) extremely similar, more so than for any other pair of congeneric elements. For example, from Table IV, we note that ZrS_3 and HfS_3 have almost identical b lattice parameters (i.e., 3.620 and 3.595 Å, respectively)[7] and equal 4+ ionic radii (0.79 Å for each compound). This means that the metal-metal overlap and ligand-field-splitting effects are similar in both compounds (ZrS_3 and HfS_3), hence resulting in roughly equivalent metal d and s conduction bands separation, widths and overlaps—hence the similarities in the vuv reflectivity spectra of the compounds of the two elements.

B. Core excitations in $HfSe_3$

It has already been mentioned that the soft x-ray reflectivity spectra of $ZrSe_3$, ZrS_3, and $HfSe_3$ were measured using the Synchrotron Radiation Facility (NINA at Daresbury Laboratory, England) as a light source. All measurements were made at room temperature. Although the soft x-ray region on NINA extended from ~8 to 30 eV, only the 8 to 24 eV part of each spectrum (see Figs. 5, 6, and 9) is shown because after 24 eV the reflectivity just tails off rapidly to zero. It is observed that for photon energies less than 14 eV, the spectra of ZrS_3 (Fig. 5), $ZrSe_3$ (Fig. 6), and $HfSe_3$ (Fig. 9) all exhibit a lot of interband transitions. But in the photon energy range 14–24 eV, all the three spectra exhibit a rapid decrease in reflectivity with increase in energy, reminiscent of the behavior of some metals (e.g., Na, K, etc.) in the ultraviolet region. This falling edge in reflectivity with increase in photon energy is the well-known plasma edge. Furthermore, from Figs. 5, 6, and 9 it is noticeable that the plasma edges for ZrS_3 and $ZrSe_3$ are relatively featureless but the plasma edge on the $HfSe_3$ vuv reflectivity spectrum exhibits two peaks at ~18 and 20 eV (a separation of ~2 eV). We shall interpret these two peaks on the atomic model which we will subsequently justify with general arguments.

According to Bearden and Burr,[21] Hf (Atomic No. $Z=72$) $4f$ levels occur at ~17.1 eV. The amount of spin-orbit splitting of W ($Z=74$) $4f$ levels is quoted as amounting to ~2.9 eV (see Ref. 21). Furthermore, x-ray photoemission work on $1T$-TaS_2 (Ref. 22) gives a spin-orbit splitting of ~1.8 eV for the Ta ($Z=73$) $4f_{7/2}$ and $4f_{5/2}$ levels. Therefore the amount of spin-orbit splitting of Hf $4f$ lies between 2.9 and 1.8 eV.

On a simple j-j coupling and one-electron approximation scheme, the excited states of Hf^{4+} ion in $HfSe_3$ will contain a spin-orbit splitting of the ground-state $4f$ levels and excited state $5d$ levels. These splittings are schematically shown in Fig. 13. Let us represent by α the transitions $4f_{5/2} \rightarrow 5d_{3/2}$ and by β the transition $4f_{7/2} \rightarrow 5d_{5/2}$. Thus α represents the atomiclike transition at ~20 eV and β the transition at ~18 eV.

We return now to discuss arguments to support the atomic interpretation of cationic core transitions. The atomic interpretation is in contrast with one-electron band theory. On the one-electron band theory one would expect that (i) since

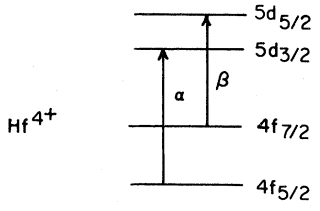

FIG. 13. A schematic representation of the spin-orbit splitting of the ground state ($4f$ levels) and excited states ($5d$ levels) in Hf.

excitations are from a flat core, the spectra should reflect the density of states of the conduction band, (ii) all core spectra in the same solid should reflect the same conduction-band density of states, and (iii) optical spectra should correlate with photoemission spectra.

Kunz[23] has reviewed many spectra, chiefly alkali halides; (i) and (ii) do not appear to hold. A good instance of the noncorrelation of (iii) is given, in the case of PbF_2 and PbI_2, by Beaumont *et al.*[24] If, in the face of available data, it is argued that the failure of one electron band theory with regard to points (i) and (ii) above is due to complicated matrix element effects, then this solution is not enlightening because such matrix elements have not, to date, been satisfactorily calculated.

On the other end, in ionic solids for example, alkali halides[25] and lead halides[26] core structure resembles (ionic) atomic spectra and is fairly invariant from compound to compound. It is not surprising that in the case of cations, transitions are atomic because of the strength not only of the ionic charge, but also of the hole which localizes the excited state on the ion.[27] It is worth noting that atomic transitions imply that the Madelung potential is similar for the excited states as well as for the ground state.[26] In the case of anions, the argument for atomiclike core excitations is less clear. It is probable that charge is transferred from the anionic core ground state onto the surrounding cations in a way analogous to the strong excitons produced by charge transfer at the fundamental edge in alkali halides. Structure is sometimes observed in solids and ascribed to anionic cores.[28] However, such structure cannot be compared with the atomic structure because negative ions are unstable in the vapor state so that negative ionic transition energies would be difficult to measure.

For these general reasons, since Hf is a cation, we expect it to behave the same way as Pb in PbF_2 (Ref. 26). We, therefore, have interpreted, as stated earlier, the two peaks on the $HfSe_3$ plasma edge as due to core excitations between Hf $4f$ and $5d$ states.

C. Dichroism in $ZrSe_3$-type crystals

Because of their monoclinic symmetry, $ZrSe_3$-type compounds are expected to exhibit different reflectivity features for $\vec{E} \perp \hat{b}$ and $\vec{E} \parallel \hat{b}$ orientations, an effect termed dichroism. In the visible region, ZrS_3 and HfS_3 have been reported to exhibit this effect.[9] This effect was investigated in these compounds using both the partially polarized vuv light (at the Cavendish) and the polarized soft-x-ray source (at Daresbury) and no dichroism was observed in any of the compounds. This apparent lack of dichroism, at high photon energies, in these MX_3 compounds should not be interpreted as implying that $\vec{\epsilon} \perp \hat{b}$ is equal to $\vec{\epsilon} \parallel \hat{b}$. We believe that this lack of dichroism in these compounds is a result of the lack of single crystallinity in the type of samples we used in our experiments. A truly single crystalline sample of these compounds would be just one strip or platelet, but such a tiny sample would be physically impossible to work with in a reflectivity experiment. A stack of platelets (all "parallel" and arranged in layers) was the way the crystals grew. But, although the platelets (crystallites) appeared parallel, to the naked eye, on the surface of the crystal, it is conceivable that as one goes deep into the crystals (along the c axis of the stack of platelets), there would be twinning on the [001] direction, as has been reported.[1] At high photon energies (vuv region), the penetration depth is larger than at low photon energies (in the visible region); therefore, the effect of the presence of twinning would be felt more at high photon energies than at low energies. We therefore attribute (partly) the apparent lack of dichroism in these MX_3 compounds at high photon energies, to the polycrystallinity-like nature of the crystals used for this work. Possibly, a single strip crystal of these compounds would exhibit dichroism in the whole range of the optical spectrum. However, it is worth mentioning that a thorough literature survey seems to indicate that no one has so far managed to observe high-energy dichroism in crystals—the work of Olson and Lynch[29] on CdO is a good example. Dichroism seems to be an effect easily observable 3-4 eV above the Fermi level of a material, but this effect washes out (apparently) as one excites electrons from deep in the valence band. The reasons for this high-energy "wash out" of dichroism in crystals are not yet clear. We intend to make a fuller investigation of dichroism in these ZrS_3-type materials at a latter stage.

IV. CONCLUSION

The vacuum ultraviolet reflectivity spectra of the trisulphides, triselenides, and tritellurides of Ti (except the hitherto unreported $TiSe_3$ and $TiTe_3$), Zr, and Hf have been measured, and the gross features interpreted using simple physical and chemical arguments. As a result of this study, simple (speculative) band-structure models for TiS_3; ZrS_3, HfS_3 and ZrX_3 or HfS_3 (where X = Se, Te) have been proposed. Because of its wide valence bandwidth,[10] interband transitions in ZrS_3 are believed to be determined by the valence-

band density-of-states distribution whereas interband transitions in all other Group IVA trichalcogenides are probably determined by conduction-band density-of-states distribution because of their relatively narrow valence band (~6 eV in $ZrSe_3$).[20] The striking difference between the Zr or Hf materials and TiS_3 arises largely from the smaller size of the Ti 4+ ion (0.61 Å 4+ ionic radius)[30] and the corresponding reduction of the effect of the ligand field on the Ti d orbitals. The similarities between the spectra of Zr and Hf trichalcogenides are due (i) to the lanthanide contraction effect on the periodic table and (ii) to their structural isomorphy.

It must be emphasized that the schematic band-structure models for the Group IVA trichalcogenides presented in this paper are still speculative and incomplete at this stage. Theoretical band-structure calculations on these complicated systems are long overdue. Furthermore, on the experimental front, infrared and visible regions reflectivity data on these $ZrSe_3$-type materials are needed (in addition to the vuv reflectivity data presented here) in order to enable a Kramers-Kronig analysis (to obtain $\tilde{\epsilon}_1$ and $\tilde{\epsilon}_2$) of the data of these materials. The exact position of the d levels in the band structure of these materials will be determined from angle-resolved photoemission studies which are currently planned. In our band models, we tentatively placed the d_{z^2} and other d bands below $p(X-X)^*$ antibonding states. Angle-resolved photoemission work on these materials will determine the exact dispersion of the d bands in these materials. From our study, one point seems to be clear: The $ZrSe_3$-type materials have dimerized main conduction [this band consists of $p(X-X)$ antibonding states and $d(M)$ orbitals] and valence [this consists of $p(X-X)$ bonding states and $p(X)$] bands. The plasmonlike feature at ~8 eV on TiS_3 we have observed in this work can only be verified by energy loss measurements on this material.

ACKNOWLEDGMENTS

This work was supported in part by the U. S. Department of Energy, Contract No. W-7405-Eng-82, Division of Materials Sciences, budget Code No. AK-01-02-02-2. One of us (F.S.K.) would like to thank the following for financial support: (i) the Association of Commonwealth Universities in London and (ii) Trinity College, Cambridge, England. Furthermore, we would like to thank Dr. D. W. Bullett (Cavendish), Professor Fred Brown (Illinois, U. S. A.), and Dr. H. Myron (Katholieke University, Holland) for many stimulating and illuminating discussions and comments.

*Present address: Ames Laboratory-USDOE and Department of Physics, Iowa State University, Ames, Iowa, 50011.

[1]W. Kronert and K. Plieth, Z. Anorg. Allg. Chem. 336, 207 (1965).
[2]S. D. Hamann, Aust. J. Chem. 11, 391 (1958).
[3]F. K. McTaggart and A. D. Wadsley, Aust. J. Chem. 11, 445 (1958).
[4]J. A. Bear and F. K. McTaggart, Aust. J. Chem. 11, 458 (1958).
[5]F. K. McTaggart, Aust. J. Chem. 11, 471 (1968).
[6]L. Brattas and A. Kjekshus, Acta Chem. Scand. 25, 2783 (1973).
[7]H. Haraldsen, A. Kjekshus, E. Røst, and A. Steffensen, Acta. Chem. Scand. 17, 1283 (1963).
[8]H. G. Grimmeiss, A. Rabenau, H. Hahn, and P. Neiss, Z. Elektrochem. 65, 776 (1961).
[9]W. Schairer and M. W. Shafer, Phys. Status Solidi A 17, 181 (1973).
[10]F. Jellinek, R. A. Pollak, and M. W. Shafer, Mater. Res. Bull. 9, 845 (1974).
[11]D. E. Eastman and J. J. Donelon, Rev. Sci. Instrum. 41, 1648 (1970).
[12]H. P. Hughes, Ph. D. thesis, University of Cambridge, 1974 (unpublished).
[13]H. P. Hughes and W. Y. Liang, J. Phys. C 7, 1023 (1974).
[14]K. Codling, Rep. Prog. Phys. 36, 541 (1973).
[15]A. J. Bourdillon, Ph. D. thesis, University of Oxford, 1975 (unpublished).
[16]H. P. Hughes and W. Y. Liang, J. Phys. C 10, 1079 (1977).
[17]L. H. Ahrens, Geochim. Cosmochim. Acta 2, 155 (1952).
[18]L. Pauling and M. Huggins, Z. Kristallogr. 75, 128 (1934)
[19]L. Pauling, *The Nature of the Chemical Bond*, 3rd ed. (Cornell University, Ithaca, New York, 1960).
[20]D. W. Bullett, J. Phys. C 12, 277 (1979).
[21]J. A. Bearden and A. F. Burr, Rev. Mod. Phys. 39, 1, (1967); 39, 125 (1967).
[22]H. P. Hughes and R. A. Pollak, Philos. Mag. 34, 6 1025 (1976); 34, 1025 (1976).
[23]A. B. Kunz, Phys. Rev. B 12, 5980 (1975).
[24]J. H. Beaumont, A. J. Bourdillon, and J. Bordas, J. Phys. C 10, 333 (1977).
[25]S. T. Pantelides, Phys. Rev. B 11, 2391 (1975).
[26]A. J. Bourdillon, F. S. Khumalo, and J. Bordas, Philos. Mag. B 37, 6 (1978); 37, 731 (1978).
[27]A. B. Kunz, J. Phys. C 7, L231 (1974).
[28]F. C. Brown, Phys. Rev. B 2, 2126 (1970).
[29]C. G. Olson and D. W. Lynch, Phys. Rev. B 9, 3159 (1974).
[30]R. D. Shannon and C. T. Prewitt, Acta Crystallogr. B 25, 925 (1969).